Site-specific parabolic trough collector geometry optimization based on annual energy yield

Gonzalo López[1], Ezequiel Cardozo[1], Germán Morales[1], Juan M. Rodríguez[2] and Santiago Correa[1]

1 Facultad de Ingeniería - Universidad de la República, Montevideo (Uruguay)

2 Laboratorio de Energía Solar – Universidad de la República, Salto (Uruguay)

Abstract

This work presents a methodology to optimize the geometry of parabolic trough collectors (PTCs) for site-specific applications, aiming to maximize the annual thermal output under local climatic, operational, and manufacturing constraints. Using typical meteorological year (TMY) datasets as climatic inputs, the proposed framework relies on a self-developed optical–thermal model implemented in MATLAB to evaluate combinations of mirror, receiver, and cover-tube geometries. The optimization process accounts for geographical variability, manufacturing tolerances, and material availability, enabling adaptive designs suited for regional production capabilities. This study constitutes an intermediate step of an ongoing effort aimed at developing an open-access optimization platform for parabolic trough collector design. Accordingly, the results discussed herein should be regarded as preliminary, yet they provide a consistent validation of the underlying methodology and illustrate its practical potential.

Keywords: parabolic trough collector, geometry optimization, typical meteorological year, thermal modelling

1. Introduction

Although significant research has focused on adapting CSP systems to local irradiance and climatic variability, parabolic-trough collector geometry has largely remained an off-the-shelf solution. A modest contribution is presented toward rethinking the current approach by embedding site-specific meteorological data into the mirror and receiver-cover geometry optimization process for maximum annual energy output. Moreover, locally available materials and manufacturing processes can limit design options, therefore a PTC tailored to its region's needs and resources can maximize economic and social benefits by developing domestic value chains (IRENA, 2025) as well as reducing procurement complexity.

Recent studies of PTCs typically fall into two distinct tracks: optical-only vs thermal/exergetic optimization. On the optical side, Hoseinzadeh et al. (2018) varied key geometric parameters aiming to optimize concentration ratios and intercept factors, but did not couple these results to a thermal model. On the other hand, Kasem (2022) framed the multi-objective problem to maximize thermal and exergetic efficiencies across several working fluids and inlet temperatures, while covering geometry in a limited way and without an optical optimization analysis. Unlike previous studies, the present work integrates both optical and thermal aspects into a unified optimization framework. In this study, the design variables rim angle, receiver-tube diameter, and glass-envelope diameter govern the collector's geometry and therefore determine its optical efficiency, which is then coupled with TMY data. The combination of optical response and climatic input allows the thermal model to simulate the performance of the collector, yielding the annual heat output for a given operation point (fluid inlet temperature and flow).

This work constitutes an intermediate step of an ongoing effort aimed at developing an open-access optimization platform for parabolic trough collector design. Accordingly, the results discussed herein should be regarded as preliminary, yet they provide a consistent validation of the underlying methodology and illustrate its practical potential. This article proposes a methodology to optimize the geometry of PTCs for site-

specific applications, aiming to maximize the annual thermal output under local climatic, operational, and manufacturing constraints. Using TMY datasets as climatic inputs, the framework relies on a self-developed optical-thermal model implemented in MATLAB to evaluate combinations of mirror, receiver, and cover-tube geometries. The optimization process accounts for geographical variability, manufacturing tolerances, and material availability, enabling adaptive designs suited for regional production capabilities.

The paper is organized into four main sections. Section 2 presents the methodological framework, including the optical–thermal model developed to estimate the performance of non-evacuated parabolic trough collectors and the optimization procedure used to identify optimal geometries under different operating and climatic conditions. Section 3 reports and analyzes the results obtained for representative locations, highlighting the influence of inlet temperature, flow velocity, and local meteorology on the collector's performance. Section 4 discusses the main conclusions drawn from the study and outlines potential future developments toward the creation of an open-access optimization tool.

2. Methodology

This section outlines the study's methodological framework. Section 2.1 introduces an optical–thermal model to assess the performance of PTCs with non-evacuated receiver tubes for intermediate-temperature applications. Subsection 2.2 details a geometry-optimization procedure which consists of running simulations using the optical thermal model, incorporating typical site climate data (TMY datasets), and testing different geometries to determine the collector configuration that maximizes annual net energy generation.

2.1. Optical-thermal model

The optical model developed in MATLAB simulates the radiation transfer and concentration process in a PTC of given optical properties and manufacturing tolerances by estimating the fraction of direct normal irradiance (DNI) that is absorbed by the receiver surface, given by the expression:

$$G_{abs} = \eta_{opt}\, G_{\perp} \qquad \text{(eq. 1)}$$

where $G_{\perp} = DNI\, \cos(\theta_i)$ is the irradiance normal to the PTC's aperture at an incident angle θ_i.

The optical efficiency (η_{opt}) is obtained as the product of mirror reflectivity, receiver absorptivity, glass transmissivity, the intercept factor (γ), which itself depends on the rim angle (ψ) and the incidence angle modifier (K) which adjust the optical properties at normal irradiance when subject to non-perpendicular irradiance.

$$\eta_{opt} = K(\theta_i) \cdot \gamma \cdot (\alpha\tau\rho)_i \qquad \text{(eq. 2)}$$

An incidence angle modifier was incorporated using the empirical expression based on the Sandia Hexcel PTC (Gaul and Rabl, 1979), which has similar dimensions as the expected design case use. The used expression for the incidence angle modifier is as follows:

$$K(\theta_i) = 1 - 6.74 \times 10^{-5}\, \theta_i^2 + 1.64 \times 10^{-6}\, \theta_i^3 - 2.51 \times 10^{-8}\, \theta_i^4 \qquad \text{(eq. 3)}$$

The intercept factor (γ) accounts optical for the losses attributable to imperfections of the involved surfaces, as well as the geometrical deviations, quantifying the fraction of reflected rays that successfully strike the receiver as per the comprehensive optical analysis done by Güven and Bannerot (1986). These random and systematic errors are heavily dependent on the design's geometric tolerances and were estimated for local manufacturing capabilities as summarized in Cardozo et al. (2024). Random deviations (σ = 8.5 mrad) represent surface irregularities and local misalignments, whereas systematic deviations (β = 17.5 mrad) account for slope, tracking and assembly inaccuracies. The selection of these errors aligns with the local fabrication context discussed in this work, as it reflects achievable tolerances for low-cost, small-scale collector manufacturing.

Overall, this optical model provides a realistic yet computationally efficient representation of the solar concentration process in PTCs manufactured under non-industrial tolerances.

Taking the absorbed irradiance G_{abs} as an input for the thermal model, the useful power is related to the thermal efficiency by the equation:

$$Q = \eta_{th}\, G_{abs}. \qquad \text{(eq. 4)}$$

The power extracted by the PTCs is estimated by solving energy balance and heat transfer equations along the receiver tube, assuming a uniform circumferential flux. This approach neglects radial variations in heat flux intensity, which is acceptable for engineering-scale simulations but limits the representation of circumferential temperature gradients. Specifically, the system is discretized into n control volumes along the length of the tube, with each element solving the steady-state energy balance for each system component (water, receiver, glass, and air), and accounting for heat transfer exchanges with the ambient air using appropriate correlations according to the nature of the heat transfer (conductive, convective, and radiative). The global energy balance for each node is solved through an iterative loop that updates the local temperatures until convergence of 10^{-4} K is achieved.

Empirical correlations were used for the convective coefficient for water as the working fluid while the external convection coefficient is based on forced flow at 5 m s^{-1} wind velocity. For the annular space between the receiver and glass cover, heat transfer occurs through a combined natural convection and radiation coupling. Thermal radiation between the absorber and the glass envelope is solved using the linearized Stefan–Boltzmann formulation. The model uses fixed material properties for borosilicate glass as the cover tube, while the receiver tube retains all thermal properties of stainless steel. Its optical characteristics were assigned based on a locally available selective coating, with absorptivity and emissivity values considered as input parameters. Since the model is fully parametric, these optical properties can be readily adjusted to represent any selective coating of preference, allowing straightforward adaptation to different materials or manufacturing contexts.

The overall efficiency is then defined as:

$$\eta = \eta_{opt} \cdot \eta_{th} = \frac{\dot{m}\, c\, (T_{out} - T_{in})}{A\, DNI\, \cos(\theta_i)}, \qquad \text{(eq. 5)}$$

where the aperture area is obtained using the PTC's length and aperture width derived from the geometric rim angle relation. A comprehensive discussion of the model's mathematical formulation, assumptions, and parameter correlations can be found in Cardozo et al. (2024). The resulting framework is comparable in scope to Kalogirou et al. (1997) analytical model PTCDES but differs in its modular MATLAB implementation that allows systematic parameter optimization.

The optical–thermal model was validated using the experimental data reported by Evans and Matthews (1996), who studied the performance of a parabolic trough collector under steady-state conditions. The validation focused on comparing the predicted and experimental overall efficiencies for equivalent operational parameters, including incident irradiance, mass flow rate, and inlet temperature. The resulting deviation between simulated and measured temperatures remained below 3% for most operating points, confirming the model's ability to accurately reproduce the collector's thermal behavior. This agreement demonstrates that the simplifications introduced—such as the one-dimensional formulation of the energy balance and the assumption of uniform heat flux along the receiver circumference—are acceptable within the operational range of interest. Although the model neglects certain effects such as circumferential heat flux variations, end losses, and dynamic transients, it provides an adequate trade-off between computational simplicity and predictive accuracy for design-oriented applications. Consequently, the model was deemed suitable for use in the subsequent parametric optimization of receiver geometries and operating conditions.

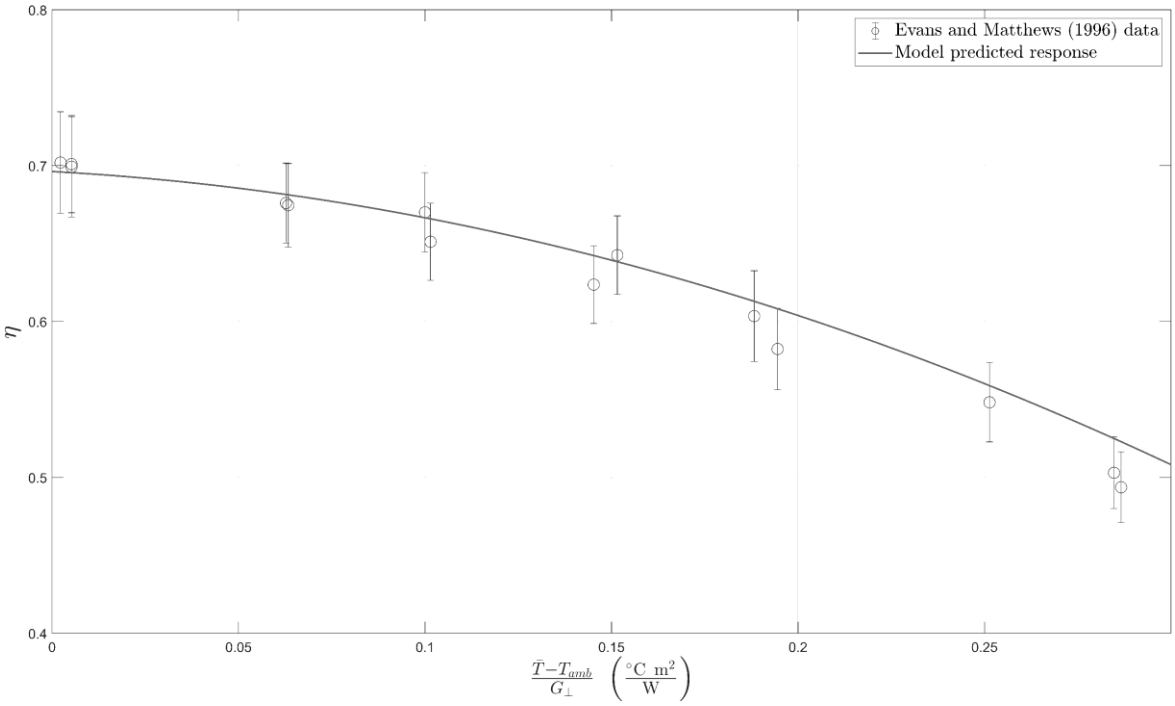

Figure 1: Predicted and experimental overall efficiencies for the PTC studied by Evans and Matthews (1996). The model prediction falls within the experimental uncertainty for all except one datapoint.

2.2. Geometry optimization algorithm

The optimization problem is formulated as a mixed-variable optimization whose objective is to maximize heat generation while keeping hydraulic pumping losses at a minimum. Thus net energy (E_{net}) was the performance indicator (PI) chosen as the objective function, defined as the extracted heat minus the electric energy required by the pumping system to recirculate water, given by the expression:

$$E_{net} = Q - \frac{\dot{V}\,\Delta P}{\eta_{pump}} \qquad \text{(eq. 6)}$$

The hydraulic subsystem is modeled to estimate annual pumping power losses through the Darcy–Weisbach equation, corrected by a typical pump efficiency of $\eta_{pump} = 35\%$.

The problem formulation considers both continuous and discrete design parameters. The rim angle (ψ) is treated as a quasi-continuous variable and is evaluated in discrete increments of one degree to provide adequate resolution while maintaining computational efficiency. Conversely, the receiver tube and glass envelope diameters are treated as discrete variables, as these correspond to standard, commercially available sizes presented on Table 1. This distinction reflects realistic manufacturing constraints and ensures that the optimization outcomes are directly applicable to practical design and procurement processes.

Table 1: Commercially available reflective sheet metal, receiver and glass cover tubes considered for the collector design.

Reflective sheet	Receiver tube (RT)	Cover tube (CT)
Anodized aluminium 2 m x 4 m.	DN 32, DN 40, DN 50, DN 65.	Outer diameters (mm): 54, 56, 58, 60, 65, 70, 75, 80, 90, 95, 100, 105.
$\rho = 0.84$	AISI 304 / SCH 5s	Borosilicate glass / ~ 5 mm thick

The available sheet metal width imposes a practical limitation on the collector chord length, thus determining the maximum aperture area attainable for a given rim angle. The optimization problem underlying the geometry selection of the parabolic trough collector constitutes a solution of compromises. A smaller rim angle produces

a flatter parabola, increasing the aperture and decreasing the intercept factor (γ) since mirror slope and alignment errors become more detrimental leading to rays diverging further from the focal region. Increasing the receiver tubes outer diameter has a positive impact on the intercept factor (γ), since the target area where reflected radiation is absorbed gets effectively larger. On the other hand, larger receiver tube area leads to higher thermal losses, lowering the collector's thermal efficiency (η_{ter}). Both examples represent the interdependency of variables and the balance solution required in order to find an optimal solution.

The algorithm employs an exhaustive or brute-force search strategy, evaluating all feasible geometric combinations within the defined parametric space. Each candidate configuration is subject to feasibility criteria ensuring physical consistency, most notably, that the receiver tube fits within the glass envelope. For each valid configuration, the optical–thermal model described previously is executed under the range of climatic and operational conditions.

A simulation cycle begins by importing site TMY data obtained from Climate.OneBuilding (2025), using the standard EPW format. The Climate.OneBuilding project offers a vast repository of worldwide TMYs with consistent structure, thus ensuring results' comparability.

The imported data is first filtered to only consider daylight datapoints (DNI > 0) followed by a binning process. This step consists in using irradiance–temperature histograms to obtain characteristic bin centers of irradiance normal to the aperture ($G_{\perp}$) and ambient temperature (T_{amb}). For each bin, the optical-thermal model obtains heat and net energy yield estimates based on the bin center values. Then, these values are multiplied by the number of hours within the bin (counts) and the process is repeated for all bins with non-zero counts, thus obtaining the annual heat and net energy yields.

The selected binning is based on the discretization into 6 ambient temperature and 15 irradiance ranges. This binning approach allowed for significant reductions in computational time while preserving the representativeness of climatic variability. Therefore, the chosen configuration of 90 bins was selected as the baseline for the subsequent analyses, representing an optimal balance for iterative parametric studies and tool development.

The dataset resulting from the binned simulation, which includes the annual net energy output for every feasible combination of rim angle, receiver diameter, and glass envelope diameter, is subsequently analyzed to identify the configuration that maximizes net annual energy generation for the given location and operating point.

To illustrate the implementation of the algorithm, assess the influence of different variables, and establish practical guidelines for its use, the optimization routine was executed for several representative cases. These included variations in the binning resolution, geographical location, and operating conditions (e.g., inlet temperature and mass flow rate).

The results and conclusions derived from these simulations are presented in Section 3.

3. Results

This section presents the results of the optimization framework applied to different operating and climatic conditions. The first subsection illustrates the typical outputs of the model, exemplified with an optimization ran for Montevideo for an operating point of flow velocity $v = 1$ m s^{-1} and inlet temperature $T_{in} = 100$ ºC. The ensuing subsection studies the optimal geometry's sensitivity to three factors: binning strategy, operating point and location. Through these analyses, the section aims to summarize the main capabilities and outputs of the optimization process.

3.1. Illustrative Optimization Case

The optimization process produces several outputs that provide an insight into the climate of the studied location, the inner workings of the exhaustive search method as well as the predicted performance for the

optimal PTC geometry. These results are presented through four representative figures (Figures 2-4), which collectively illustrate the steps taken on the optimization routine. The following are the results of an optimal geometry search ran for a PTC located in Montevideo operating with water at a mean flow velocity of $v = 1$ m s^{-1} and inlet temperature $T_{in} = 100$ ºC.

The first graphical output, shown on Figure 2, corresponds to the two-dimensional histogram of climatic conditions derived from the TMY dataset. This histogram is constructed according to the binning strategy detailed in Subsection 2.2, where the annual ambient temperature and irradiance normal to the aperture data are discretized into defined intervals. The resulting plot provides a visual representation of the typical climate profile for the location under study, highlighting the most frequent operating conditions throughout the year and allows for the identification of dominant climatic seasons, such as high-irradiance summer conditions and lower-temperature winter operations. This information serves as a foundation for the subsequent weighting of performance calculations in the optimization framework.

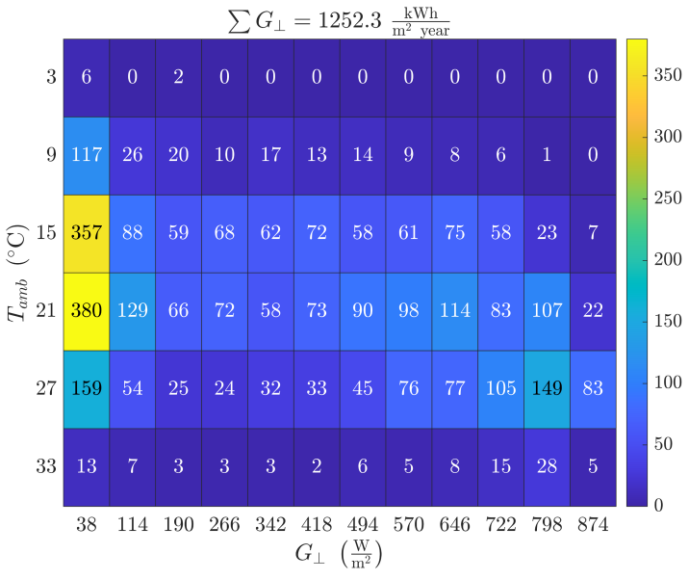

Figure 2: Irradiance normal to the aperture and ambient temperature histogram for Montevideo's TMY, each bin is defined by its center values and contains the count of hours within its boundaries. See that the annual irradiance normal to the aperture is provided as a summary of the location's solar resource availability.

The second output of interest, is the estimated annual net energy generation (the objective function of the optimization process) for all feasible combinations of rim angle, receiver tube and glass envelope. Figure 3.a presents all feasible combinations into a graph where each point corresponds to a simulated configuration, highlighting the rim angle and receiver tube size's effect on annual net energy generation. The surface of results forms distinct point clouds, where elongated clusters of data can be distinguished. These clusters correspond to groups of simulations sharing the same receiver geometry. Within each cluster, variations in glass-envelope diameter have a limited impact on annual heat output, suggesting that the optical-thermal sensitivity to envelope diameter is considerably lower than that associated with receiver diameter or rim angle. The visualization thus provides an intuitive overview of the design space, indicating which geometrical combinations yield the highest annual energy capture.

A similar trend is observed in the third output, Figure 3.b, which depicts the annual overall efficiency. When employed together with the annual irradiance normal to the aperture, this variable allows the user to extract an annual heat generation for a given operational point. The resulting plot maintains a form comparable to that of the annual net energy generation but with reduced penalization for small diameter receiver tubes, reflecting the influence of hydraulic losses on the objective function. Aside from the less distinct yet evident clustering behavior, a common trend which appeared for all optimization processes run is the smoothness of the results. This ensures that, for a given receiver and glass cover tube combination, small rim angle variations have negligible impact on the PTC's performance. This indicates that moderate adjustments to rim angle motivated by structural or manufacturing considerations can be implemented without substantially affecting the collector's overall efficiency or annual energy output.

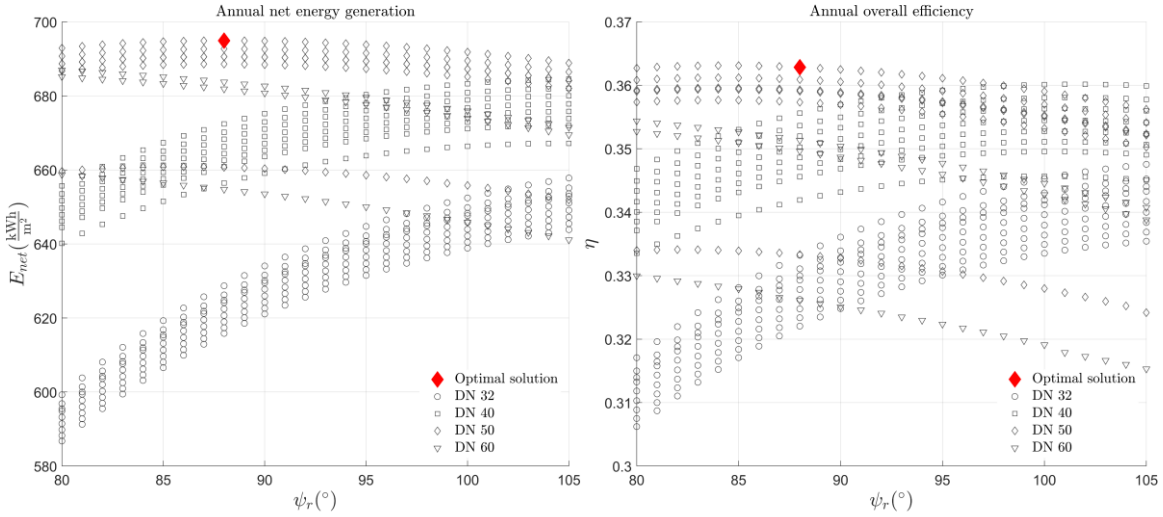

Subfigure 3.a: Annual net energy for all candidate geometries.

Subfigure 3.b: Annual overall efficiency for all candidate geometries.

Figure 3: Comparison of the annual net energy output (left) and annual efficiency (right) obtained from the optimization for Montevideo. Each point represents the expected annual performance of one candidate geometry.

Finally, Figure 5 presents the optimization tool's user with the expected performance curve of the optimal solution. Regardless of the error expected from a theoretical estimate, this output serves the purpose of evaluating the optimal PTC's response for a wide range of operation points, which is condensed into a quadratic regression as per ISO 9806 (2025) recommendation. The independent term of this expression represents the optical efficiency (η_{opt}) of the optimal solution.

Overall, these observations underscore the robustness of the optimization framework and its capacity to identify stable, well-defined optima within the design space. The visualization of all feasible combinations enables the identification of geometric families that not only maximize performance but also exhibit limited sensitivity to minor deviations in design parameters, a desirable characteristic for practical engineering applications. Moreover, the tool provides the user with an understanding of the selected location's climate and the bins used, as well as insight into the candidate geometries assessment and a reasonable estimate of the performance of the optimal geometry.

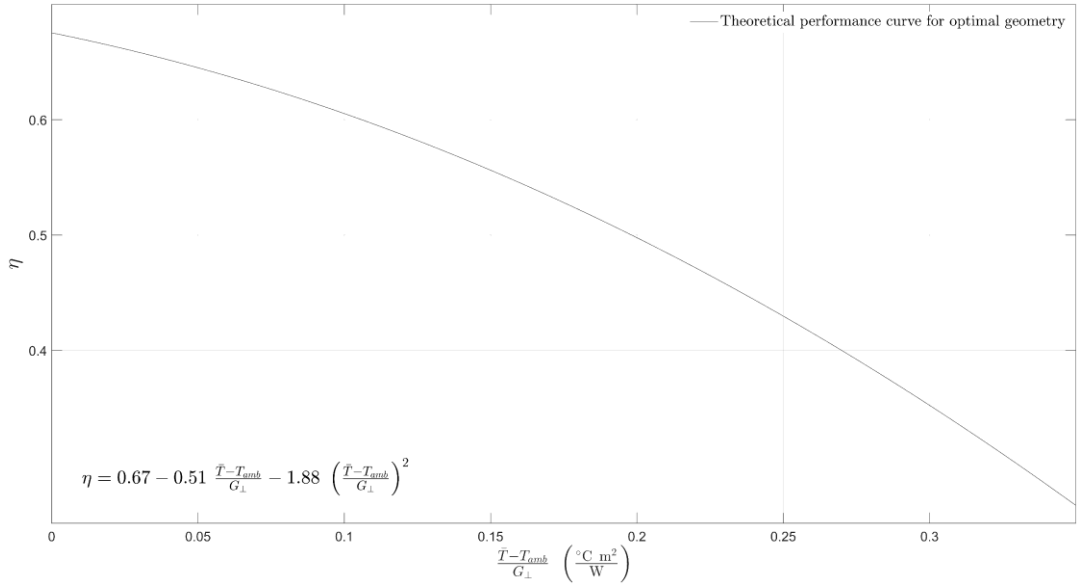

Figure 4: Theoretical performance curve for the optimal geometry for a PTC located in Montevideo operating at a mean flow velocity of v = 1 m s^{-1} and inlet temperature of 100 ºC.

3.2. Sensitivity analysis

Binning:

In order to find an acceptable binning strategy, a sensitivity analysis was conducted to quantify the trade-off between accuracy and computational demand. Using as a reference Montevideo's TMY datapoints corresponding to daylight hours, several optimization processes with varying numbers of bins were conducted and benchmarked against the reference approach. The binning strategy aims to reduce the number of simulations required to obtain the annual output of a candidate PTC from approximately 4300 to, at most, the number of bins within the data is sorted. Figure 2 shows the relative error on the expected annual heat output as well as the relative computation time resulting from the comparison with the reference values obtained from the non-binned data.

The results from the optimization show that the deviation in predicted annual heat output is below 1.5% for the 15x6-bin configuration, with a reduction in computation time of two orders of magnitude. Increasing the resolution to 300 bins yielded marginal accuracy improvements (<1%) while substantially increasing the processing time, which follows a pseudo-linear relationship with bin number on the 1-900 bin range. Similar analysis carried out for Calama and Fortaleza show an asymptotic behavior with an overall tendency to overestimate the annual heat output. Consequently, the 90-bin configuration was selected as the baseline case for the following optimization analyses, representing an optimal balance between numerical accuracy and computational efficiency.

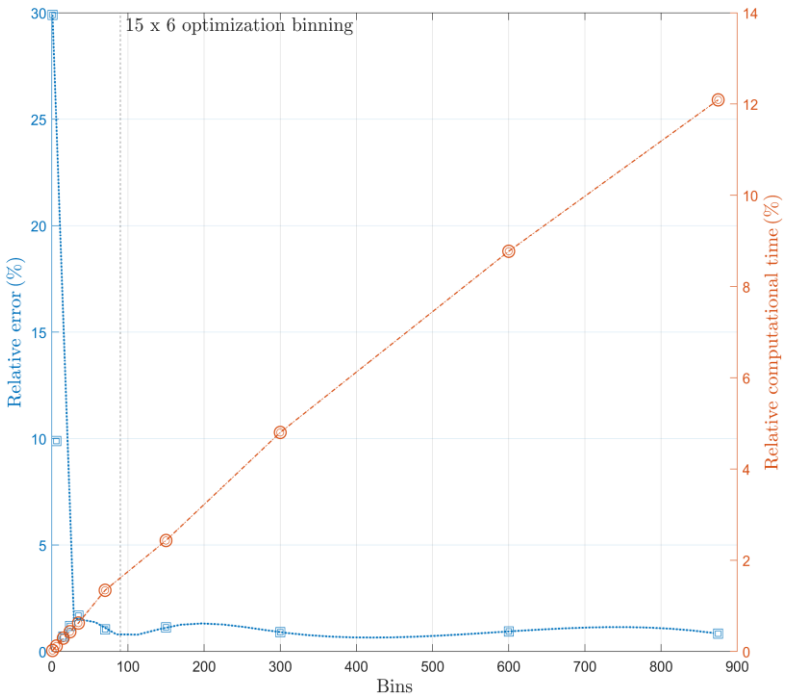

Figure 5: Relative error and relative computation time as a function of the number of bins used to summarize TMY data. See that the adoption of a 15 x 6 binning strategy grants a relative error of less than 1,5% whilst taking less than 1% of the computing time required for a non-binned approach.

Operating point:

Table 2 summarizes the optimal geometric configurations obtained for a series of parametric optimizations carried out at different combinations of inlet fluid temperature (from 80 °C to 180 °C) and mean flow velocity (from 0.15 m s^{-1} to 2.5 m s^{-1}). All simulations correspond to the same geographical location—Montevideo, Uruguay—and were conducted using identical optical, thermal, and environmental parameters. Therefore, the observed trends arise exclusively from variations in operating temperature and flow velocity.

Table 2: Optimal solutions for operational points in Montevideo.

	0.15 m s^{-1}			0.6 m s^{-1}			1.1 m s^{-1}			1.5 m s^{-1}			2 m s^{-1}			2.5 m s^{-1}		
	ψ (º)	RT	CT	ψ (º)	RT	CT	ψ (º)	RT	CT	ψ (º)	RT	CT	ψ (º)	RT	CT	ψ (º)	RT	CT
80ºC	91	DN50	85 mm	91	DN50	85 mm	91	DN50	85 mm	90	DN50	85 mm	89	DN50	85 mm	87	DN50	85 mm
90ºC	89	DN50	85 mm	89	DN50	85 mm	89	DN50	85 mm	88	DN50	85 mm	87	DN50	85 mm	87	DN50	85 mm
100ºC	88	DN50	85 mm	88	DN50	85 mm	87	DN50	85 mm	87	DN50	85 mm	87	DN50	85 mm	85	DN50	85 mm
110ºC	87	DN50	85 mm	87	DN50	85 mm	87	DN50	85 mm	87	DN50	85 mm	85	DN50	85 mm	102	DN40	70 mm
120ºC	85	DN50	85 mm	85	DN50	85 mm	85	DN50	85 mm	85	DN50	85 mm	85	DN50	85 mm	101	DN40	70 mm
130ºC	85	DN50	85 mm	85	DN50	85 mm	85	DN50	85 mm	84	DN50	85 mm	101	DN40	70 mm	100	DN40	70 mm
140ºC	84	DN50	85 mm	84	DN50	85 mm	84	DN50	85 mm	83	DN50	85 mm	100	DN40	70 mm	99	DN40	70 mm
150ºC	83	DN50	85 mm	83	DN50	85 mm	82	DN50	85 mm	99	DN40	70 mm	98	DN40	70 mm	98	DN40	70 mm
160ºC	98	DN40	70 mm	98	DN40	70 mm	98	DN40	70 mm	98	DN40	70 mm	98	DN40	70 mm	97	DN40	70 mm
170ºC	98	DN40	70 mm	98	DN40	70 mm	98	DN40	70 mm	97	DN40	70 mm	97	DN40	70 mm	96	DN40	70 mm
180ºC	97	DN40	70 mm	97	DN40	70 mm	97	DN40	70 mm	96	DN40	70 mm	96	DN40	70 mm	95	DN40	70 mm

The results reveal clear and consistent trends in how the optimal geometry evolves with the operating point. The first general pattern concerns the rim angle (ψ), which exhibits a progressive decrease as the inlet temperature increases. This indicates that at higher operating temperatures, wider parabolas (i.e., smaller rim angles) and consequently larger aperture areas yield higher annual heat outputs. Physically, this trend can be interpreted as a preference for maximizing the collector's ability to capture solar radiation rather than maintaining a high intercept factor, illustrating a fundamental design trade-off between optical precision and energy collection area.

A second important pattern concerns the receiver tube diameter. As the inlet temperature increases, the optimization consistently identifies smaller receiver diameters as optimal. This inverse relationship reflects the strong influence of temperature-dependent thermal losses. Since radiative and convective heat losses scale with surface area, reducing the receiver diameter minimizes the total heat loss for a given absorbed flux. This becomes particularly important at higher temperatures, where radiative losses (which scale with T^4) dominate. At low operating temperatures, the penalty associated with larger surface area is comparatively small, allowing for larger receiver tubes that improve optical interception and decrease head loss.

A third key observation is that the cover tube diameter consistently varies in tandem with the receiver diameter. The results show a clear pairing between specific receiver and cover diameters: for example, a DN 50 receiver is most often coupled with a glass envelope of 85 mm, while a DN 40 receiver pairs consistently with a 70 mm envelope. This coupling arises from the combined influence of convective and radiative heat transfer across the annular space between the receiver and the glass cover. An optimal annular spacing ensures that convection remains limited while radiative exchange is effectively suppressed. If the gap is too small, the conductive term of natural convection intensifies, leading to excessive thermal losses. If it is too large, the glass cover area increases, augmenting radiative losses to the ambient as well as being at risk of developing an annular turbulent flow, which also leads to penalizing thermal losses. Therefore, the optimization identifies specific receiver–cover combinations that minimize total thermal losses for each operating condition.

The influence of flow velocity is comparatively secondary but still noticeable. As velocity increases, the optimal configurations tend to shift toward slightly larger receiver diameters, particularly at intermediate temperatures. This behavior can be attributed to the enhanced internal convective coefficient that accompanies higher flow rates. Greater turbulence inside the receiver improves heat transfer to the working fluid, which partially offsets the effect of increased heat loss from larger surfaces. However, the trend is not dominant, and the geometric choices remain primarily governed by the thermal–optical balance dictated by temperature. This result matches the analysis conducted by Kasem (2022), which highlights that flow rate has meagre impact on the optimization process. As a result of this finding, the flow rate was diregarded as an optimization variable on his work.

Location:

The optimization procedure was applied to three reference locations Calama (Chile), Fortaleza (Brazil), and Montevideo (Uruguay) selected for their diverse climatic conditions representative of cold desert climates (*BWk*), tropical wet and dry climate (Aw) and humid subtropical climate (Cfa) on Köppen-Geiger climate classification respectively.

The comparative analysis of the optimization results for Fortaleza, Calama, and Montevideo reveals how climatic conditions exert a clear influence on the collector's optimal geometry. Although the same methodology, operating parameters, and geometric constraints were applied to all three locations, the distinct irradiance-ambient temperature profiles of each site lead to systematic shifts in the optimal rim angle, receiver diameter, and cover diameter.

Overall, Calama consistently exhibits the largest rim angles, whereas Fortaleza presents the smallest of the three. This trend aligns with the solar resource characteristics of each site: Calama's high-altitude desert climate provides high direct normal irradiance (DNI) and high ambient temperatures, favoring narrow parabolas with high concentration ratios and thus smaller receiver diameters, which minimizes thermal losses. In contrast, Fortaleza's humid tropical climate combines high ambient temperatures with moderate DNI, where optical concentration becomes less beneficial compared to an aperture increase. Under these conditions, the optimization favors flatter parabolas, larger apertures with lower rim angles, so as to maximize total solar collection rather than optical precision. Montevideo, with temperate conditions and moderate DNI, yields intermediate values, confirming the model's sensitivity to local meteorological inputs. Table 3 displays the optimal geometries derived from the optimization process for operating points of inlet fluid temperature ranging from 80 °C to 180 °C and mean flow velocities from 0.15 m s^{-1} to 2.5 m s^{-1}.

Table 3: Optimal solutions for operational points in Fortaleza and Calama.

	Fortaleza									**Calama**								
	0.15 m s^{-1}			**1.1 m s^{-1}**			**2.5 m s^{-1}**			**0.15 m s^{-1}**			**1.1 m s^{-1}**			**2.5 m s^{-1}**		
	ψ (°)	RT	CT	ψ (°)	RT	CT	ψ (°)	RT	CT	ψ (°)	RT	CT	ψ (°)	RT	CT	ψ (°)	RT	CT
80°C	91	DN50	85 mm	90	DN50	85 mm	105	DN40	70 mm	95	DN50	85 mm	95	DN50	85 mm	91	DN50	85 mm
90°C	89	DN50	85 mm	88	DN50	85 mm	103	DN40	70 mm	94	DN50	85 mm	93	DN50	85 mm	90	DN50	85 mm
100°C	87	DN50	85 mm	87	DN50	85 mm	103	DN40	70 mm	92	DN50	85 mm	92	DN50	85 mm	89	DN50	85 mm
110°C	87	DN50	85 mm	86	DN50	85 mm	101	DN40	70 mm	91	DN50	85 mm	90	DN50	85 mm	88	DN50	85 mm
120°C	85	DN50	85 mm	85	DN50	85 mm	100	DN40	70 mm	89	DN50	85 mm	89	DN50	85 mm	87	DN50	85 mm
130°C	84	DN50	85 mm	84	DN50	85 mm	98	DN40	70 mm	88	DN50	85 mm	88	DN50	85 mm	87	DN50	85 mm
140°C	84	DN50	85 mm	99	DN40	70 mm	98	DN40	70 mm	87	DN50	85 mm	87	DN50	85 mm	85	DN50	85 mm
150°C	83	DN40	70 mm	98	DN40	70 mm	97	DN40	70 mm	86	DN50	85 mm	86	DN50	85 mm	85	DN50	85 mm
160°C	98	DN40	70 mm	97	DN40	70 mm	96	DN40	70 mm	85	DN50	85 mm	85	DN50	85 mm	101	DN40	70 mm
170°C	98	DN40	70 mm	96	DN40	70 mm	95	DN40	70 mm	85	DN50	85 mm	84	DN50	85 mm	100	DN40	70 mm
180°C	95	DN40	70 mm	95	DN40	70 mm	94	DN40	70 mm	84	DN50	85 mm	84	DN50	85 mm	99	DN40	70 mm

For all three sites, the rim angle generally decreases with increasing inlet temperature, with a rate of reduction seemingly independent of climate of ~ 0.1° K^{-1}. On the other hand, the receiver tube diameter (RT) follows the inverse relationship with temperature observed previously for Montevideo, but with site-specific differences in magnitude. In Calama, where the heat flux intensity is higher, larger receiver tubes (DN50) remain optimal throughout the range, ensuring sufficient interception of concentrated radiation while keeping losses acceptable due to the high ambient temperature. In Fortaleza, however, smaller receiver diameters (DN40) become preferable at higher inlet temperatures because radiative and convective losses are more severe. A consistent coupling between the receiver and cover diameters is evident in all cases. The optimization always pairs DN50 receivers with 85 mm glass envelopes and DN40 receivers with 70 mm covers. This pairing minimizes heat loss through the annular gap while maintaining manufacturable dimensions. The persistence of this relationship across climates confirms that the receiver–cover interaction is mainly governed by heat transfer physics rather than meteorological variability.

Taken together, these results highlight that climatic conditions exert a decisive influence on the geometric optimization of non-evacuated PTCs. In high-irradiance and high-temperature environments such as Calama, the optimization favors high rim angles and larger receiver diameters, which enhance optical concentration and yield the highest overall efficiencies—ranging from 0.60 to 0.45 across the tested operating points. In contrast, Fortaleza's warm and humid tropical climate promotes the selection of flatter parabolas and smaller receivers, which mitigate convective and radiative losses at the cost of optical precision. As a result, the annual thermal efficiency is lower, varying between 0.44 and 0.23. Montevideo, characterized by moderate DNI and temperate ambient conditions, exhibits intermediate behavior, with geometries that balance optical and thermal factors, and annual overall efficiencies ranging from 0.41 to 0.25 depending on the operating point.

These efficiency ranges confirm the strong coupling between collector geometry, operating conditions, and local climate. They also illustrate the versatility of the optimization tool in adapting to different meteorological

contexts while maintaining physically consistent trends across all sites. It is important to note, however, that these values should be regarded as preliminary results. The analyses are still being refined, and ongoing work aims to validate and consolidate the numerical outputs with additional simulations and sensitivity checks. Nonetheless, the current findings already demonstrate the tool's potential to support geographically adaptive PTC design, capable of tailoring collector geometries to maximize annual energy output under diverse climatic scenarios.

4. Conclusion and future work

Results

The results presented in this work summarize the performance of a geometry optimization framework for parabolic trough collectors that simultaneously accounts for optical and thermal behavior under local climatic conditions. The developed MATLAB-based model, validated against experimental data, integrates geometric variables—rim angle, receiver, and glass envelope diameters—with site-specific meteorological inputs. This coupling enables an estimation of the annual thermal output for each candidate configuration while considering hydraulic penalties and optical imperfections representative of locally manufacturable collectors.

A key contribution of this analysis lies in the type of results obtained. Traditional geometry optimization studies for PTCs have typically sought to maximize optical efficiency alone, treating the problem as purely optical and neglecting how the collector aperture limits the total intercepted irradiance. Such optical-only analyses can lead to geometries that achieve high intercept factors but do not necessarily maximize the overall solar energy captured by the collector. The present approach, by contrast, explicitly incorporates the influence of aperture size and thermal performance through the coupling of the optical–thermal model.

The results for Montevideo, Fortaleza, and Calama demonstrate consistent and physically coherent trends, confirming the model's ability to capture how solar resource availability and ambient temperature influence optimal PTC geometry. The comparative analysis highlights the importance of incorporating climate data into the design process, as optimal geometries vary significantly with local meteorological conditions. Overall, the methodology shows promise as a foundation for adaptive, site-specific PTC design.

Future Work

Whilst the optical performance in this study relies on Güven and Bannerot's (1986) established analytical formulation widely validated in the literature, future versions of the tool may integrate ray-tracing simulations to refine the estimation of intercept factors. Such hybridization would allow for a more detailed optical assessment without significantly increasing computational requirements, as the optimization is conducted for discrete operating points. These improvements will contribute to enhancing both the precision and the versatility of the framework while maintaining its accessibility and low computational cost.

This study represents a milestone in a broader effort toward the development of an open-access optimization platform for parabolic trough collectors. The ongoing work aims to extend the tool's flexibility and applicability by incorporating additional design variables and configurations. Future developments include the capability to simulate arrays of collectors operating in series and parallel arrangements, as well as integrating other tracking algorithms, incorporating transient energy storage effects, and extending the tool's capability to simulate other working fluids aside from water.

In future implementations, the optimization framework is expected to incorporate economic indicators such as the levelized cost of energy (LCOE), alongside thermal performance, enhancing its applicability for project evaluation and investment decisions.

Finally, future work will include benchmarking the optimized geometries against commercially available parabolic trough collectors, in order to evaluate how the proposed custom-made design performs relative to existing market solutions under equivalent operating and climatic conditions.

5. References

Kasem, M.M., 2022. Multiobjective design optimization of parabolic trough collectors. Scientific Reports 12:19964.

Hoseinzadeh, H., Kasaeian, A., Shafii, M.B., 2018. Geometric optimization of parabolic trough solar collector based on the local concentration ratio using the Monte Carlo method. Energy Conversion and Management. 175, 278-287.

Cardozo, E., López, G., Morales, G., 2025. Diseño y evaluación termo-económica de un concentrador cilindro-parabólico para aplicaciones industriales de media temperatura. Colibri, Universidad de la República. https://www.colibri.udelar.edu.uy/jspui/handle/20.500.12008/51985 last accessed 27/10/2025.

Güven, H.M., Bannerot, R.B., 1986. Determination of error tolerances for the optical design of parabolic troughs for developing countries. Solar Energy. Volume 36, Issue 6, 535-55.

Gaul, H., Rabl, A., 1979. Incidence angle modifier and average optical efficiency of parabolic trough collectors. Silver Jubilee International Congress of the International Solar Energy Society. Atlanta, May 28-June 1.

Solkote Selective Solar, 2025. SOLEC-Solar Energy Corp. https://solec.org/solkote/solkote-technical-specifications/ last accessed 27/10/2025.

Kalogirou, S., Lloyd, S., Ward, J., 1997. Modelling, optimisation and performance evaluation of a parabolic trough solar collector steam generation system. Solar Energy. Volume 60, Issue 1, 49-59.

Evans, L.R., Matthews, C.W., 1996. Test Results, Industrial Solar Tecnology Parabolic Trough Solar Collector. Sandia National Laboratories.

Climate.OneBuilding, 2025. https://climate.onebuilding.org/#gsc.tab=0 last accessed 27/10/2025.

International Standards Organization, 2025. ISO 9806:2025 Solar thermal collectors test methods.

IRENA, 2025. Renewable energy benefits: Leveraging local capacity for concentrated solar power. International Renewable Energy Agency, Abu Dhabi.